

# 1 Abstract

2 Persistent divergences among the predictions of complex carbon cycle models include  
3 differences in the sign as well as the magnitude of the response of global terrestrial  
4 primary production to climate change. This and other problems with current models  
5 indicate an urgent need to re-assess the principles underlying the environmental  
6 controls of primary production. The global patterns of annual and maximum monthly  
7 terrestrial gross primary production (GPP) by C<sub>3</sub> plants are explored here using a  
8 simple first-principles model based on the light-use efficiency formalism and the  
9 Farquhar model for C<sub>3</sub> photosynthesis. The model is driven by incident  
10 photosynthetically active radiation (PAR) and remotely sensed green vegetation cover,  
11 with additional constraints imposed by low-temperature inhibition and CO<sub>2</sub> limitation.  
12 The ratio of leaf-internal to ambient CO<sub>2</sub> concentration in the model responds to  
13 growing-season mean temperature, atmospheric dryness (indexed by the cumulative  
14 water deficit, ΔE) and elevation, based on optimality theory. The greatest annual GPP  
15 is predicted for tropical moist forests, but the maximum (summer) monthly GPP can  
16 be as high or higher in boreal or temperate forests. These findings are supported by a  
17 new analysis of CO<sub>2</sub> flux measurements. The explanation is simply based on the  
18 seasonal and latitudinal distribution of PAR combined with the physiology of  
19 photosynthesis. By successively imposing biophysical constraints, it is shown that  
20 partial vegetation cover – driven primarily by water shortage – represents the largest  
21 constraint on global GPP.

## 22 1 Introduction

23 Differences among model predictions of the terrestrial carbon balance response to  
24 changes in climate and atmospheric carbon dioxide concentration ([CO<sub>2</sub>]) remain  
25 stubbornly large ([Ciais et al., 2013](#); [Friedlingstein et al., 2006](#); [Sitch et al., 2008](#)).  
26 After re-analysing coupled climate-carbon cycle model results from [Friedlingstein et al. \(2006\)](#),  
27 [Denman et al. \(2007\)](#) revealed disagreements in the overall magnitude of  
28 the modelled (positive) climate-CO<sub>2</sub> feedback and also in the responses of key  
29 processes – ocean CO<sub>2</sub> uptake, soil organic matter decomposition, and especially  
30 terrestrial net primary production (NPP) – to [CO<sub>2</sub>] increase and/or climate change.  
31 Modelled positive responses of global NPP to [CO<sub>2</sub>] varied by a factor greater than  
32 five, while the models disagreed even on the sign of the response of global NPP to  
33 climate. The more recent Earth System Models (ESMs) in the Coupled Model  
34 Intercomparison Project 5 (CMIP5) archive show no better agreement ([Ahlström et al., 2012](#);  
35 [Anav et al., 2013](#); [Arora et al., 2013](#); [Friedlingstein et al., 2014](#); [Jones et al., 2013](#);  
36 [Todd-Brown et al., 2013](#)). Ciais et al. (2013) summarized the CMIP5  
37 carbon-cycle results (their Fig. 6.21) and highlighted the weak land carbon uptake  
38 response to both [CO<sub>2</sub>] and climate change shown by two ‘N-coupled’ ESMs (models  
39 allowing for interactions between the terrestrial C and N cycles). The CMIP5 models  
40 collectively show a high bias in the simulation of recent trends in atmospheric [CO<sub>2</sub>]

41 because the modelled uptake of CO<sub>2</sub> by the oceans and/or land is too small, being  
42 smallest in the N-coupled models ([Hoffman et al., 2013](#)). Several ‘offline’ N-coupled  
43 land carbon cycle models have also generated contradictory, and in some cases  
44 apparently unrealistic, responses of NPP to climate ([Thomas et al., 2013](#); [Zaehle and](#)  
45 [Dalmonech, 2011](#)). These disappointing outcomes of recent model development  
46 suggest to us that the controls of NPP, not least the role of nutrient limitations, are  
47 inadequately understood and that this is a major impediment to the development of  
48 reliable ESMs.

49 Perusal of the terrestrial ecology literature confirms that there is indeed no consensus  
50 on the controls of either GPP or NPP. Some empirical primary production models  
51 have continued to rely on correlations with mean annual temperature and precipitation  
52 ([Del Grosso et al., 2008](#)), even though the positive geographic relationship of GPP or  
53 NPP with temperature is almost certainly indirect rather than causative ([Bonan, 1993](#);  
54 [Garbulsky et al., 2010](#)). There is a strong correlation between the latitudinal gradients  
55 of photosynthetically active radiation (PAR) and mean annual temperature; PAR is  
56 the driving force of photosynthesis but also constitutes a nearly constant fraction of  
57 solar shortwave radiation, which is the driving force of the latitudinal temperature  
58 gradient. It is therefore very likely that the observed global relationships of GPP and  
59 NPP to temperature are caused at least in part by this correlation between temperature  
60 and PAR. Based on a model simulation, [Churkina and Running \(1998\)](#) assessed the  
61 relative importance of different climatic controls (temperature, water availability,  
62 PAR) on terrestrial primary production, indicating different controls or combinations  
63 of controls to be dominant in different regions. This analysis implicitly discounts the  
64 possibility that all three factors could simultaneously limit photosynthesis, and  
65 ignores the ubiquitous experimentally observed stimulation of C<sub>3</sub> photosynthesis by  
66 increasing [CO<sub>2</sub>]. It has long been established that agricultural crop production is  
67 proportional to the cumulative PAR absorbed by the crop ([Monteith and Moss, 1977a](#);  
68 [Monteith and Moss, 1977b](#)); yet [Pongratz et al. \(2012\)](#) and others have modelled crop  
69 production without considering PAR. Many models have invoked N and/or P  
70 limitations as ancillary controls on primary production; [Huston and Wolverton \(2009\)](#)  
71 went further, arguing that soil nutrients (rather than climate) *primarily* determine the  
72 global pattern of NPP. Finally, [Faticchi et al. \(2013\)](#) claimed that NPP is not controlled  
73 by photosynthesis at all, but rather by environmental constraints on growth.

74 Different explanations of the controls of terrestrial primary production are thus rife in  
75 the ecological literature. Yet the choice of model assumptions can imply radically  
76 different responses to global change ([Wang et al., 2012](#)). It is therefore time for a  
77 fundamental re-assessment of the controls of primary production. With this goal in  
78 mind, we define a conceptually very simple model for GPP. The model allows us to  
79 explore the consequences (and potentially, the limitations) of the hypothesis that *the*  
80 *primary controls on terrestrial GPP are incident PAR, green vegetation cover and*  
81 *[CO<sub>2</sub>]*. We consider first a counterfactual, continuously vegetated world in which C<sub>3</sub>  
82 photosynthesis operates at its full biophysical potential everywhere, and PAR is not  
83 attenuated by atmospheric absorption and clouds. Then we add constraints one by one.

84 The model has the form of a ‘light use efficiency’ (LUE) model (i.e. modelled GPP is  
85 proportional to absorbed PAR). However, unlike empirical LUE models, the value of  
86 LUE and its variation with environmental factors are derived from first principles,  
87 beginning with the standard model of C<sub>3</sub> photosynthesis ([Farquhar et al., 1980](#)). The  
88 derivation rests on the ‘co-limitation’ or ‘co-ordination’ hypothesis, which predicts  
89 that the photosynthetic capacity of leaves at any location and canopy level acclimates  
90 to the prevailing daytime PAR so as to be neither in excess (which would entail  
91 additional, non-productive maintenance respiration) nor less than is required for full  
92 exploitation of the available PAR. This hypothesis implies that average daily  
93 photosynthesis under field conditions is close to the point where the Rubisco- and  
94 electron transport-limited rates are equal. The co-limitation hypothesis has strong  
95 experimental support, as was recently demonstrated by [Maire et al. \(2012\)](#).

96 The LUE concept has been applied in diagnostic primary production models,  
97 including the Simple Diagnostic Biosphere Model, SDBM ([Knorr and Heimann,  
98 1995](#)), the Carnegie-Ames-Stanford Approach model, CASA ([Field et al., 1995;  
99 Potter et al., 1993](#)), the Simple Diagnostic Photosynthesis and Respiration Model,  
100 SDPRM ([Badawy et al., 2013](#)), and the widely used algorithms to estimate GPP and  
101 NPP from remotely-sensed ‘greenness’ data provided by MODIS ([Running et al.,  
102 2004](#)). (By diagnostic, we mean models that rely on remotely sensed green vegetation  
103 as an input – distinct from prognostic models that simulate vegetation cover.) A  
104 particular version of the co-limitation hypothesis was used to derive an explicit LUE  
105 formula in the strand of complex, prognostic terrestrial carbon cycle models that  
106 originated with BIOME3 ([Haxeltine and Prentice, 1996](#)) and the Lund-Potsdam-Jena  
107 (LPJ) DGVM ([Sitch et al., 2003](#)). CO<sub>2</sub> limitation can be represented in a natural way  
108 in the co-limitation framework, if the ratio of leaf-internal to ambient [CO<sub>2</sub>] ( $c_i/c_a$ ) can  
109 be specified. This is done here with the help of the ‘least-cost hypothesis’ ([Wright et  
110 al., 2003](#)), which states that the long-term effective value of  $c_i/c_a$  minimizes the  
111 combined unit costs of carboxylation (proportional to photosynthetic capacity) and  
112 transpiration (proportional to sapflow capacity). This hypothesis also has strong  
113 empirical support (Prentice et al., 2013) and provides a continuous prediction of the  
114  $c_i/c_a$  ratio as a function of environmental aridity, temperature and elevation. Our  
115 modelling approach thus does *not* require that we divide plants into functional types  
116 (PFTs) with apparently differing physiological responses, as has usually been done in  
117 complex models, and is now commonly done in models based on remote sensing as  
118 well.

119 We focus exclusively on GPP. It is probably reasonable to extrapolate the first-order  
120 results to NPP, given that on a global scale NPP is approximately a constant fraction  
121 of GPP ([Waring et al., 1998](#)) – although caution is needed because this fraction may  
122 vary ([DeLUCIA et al., 2007](#)). The fine-tuning of the NPP/GPP ratio is a separate issue,  
123 which will be considered in forthcoming work. C<sub>4</sub> and CAM photosynthesis are not  
124 modelled. For this reason, evaluation of the model results is based on data from  
125 forests, where C<sub>3</sub> photosynthesis predominates.

## 126 2 Methods

### 127 2.1 Model summary and protocol

128 The model was applied to the global land surface, excluding ice-covered regions and  
129 Antarctica, at a grid resolution of  $0.5^\circ$ . It was driven with a fixed seasonal cycle of  
130 PAR and climate. Insolation (shortwave solar radiation at the top of the atmosphere)  
131 was computed using standard methods. Half of solar shortwave radiation was  
132 assumed to be PAR. PAR was converted from energy to photon units using a  
133 conversion factor of  $4.5 \text{ MJ mol}^{-1}$ . Remotely sensed green vegetation cover data were  
134 used to derive absorbed PAR. Required climate data (mean monthly temperature,  
135 precipitation and fractional cloud cover) were derived from Climate Research Unit  
136 data (CRU TS3.1), averaged over the same period as the remote sensing  
137 measurements.

138 We first considered a hypothetical world in which PAR at the top of the atmosphere  
139 ( $\text{PAR}_{\text{toa}}$ , see more detailed calculations in Sect. A1) could be fully utilized by plants.  
140 In other words, we assumed a continuous vegetation cover, ideal temperature and  
141 moisture conditions, and a perfectly clear atmosphere containing adequate  $\text{CO}_2$  for  
142 optimal photosynthesis (Table 1). Potential GPP under these conditions is the product  
143 of  $\text{PAR}_{\text{toa}}$ , leaf absorptance ( $a$ ), and the intrinsic quantum efficiency of photosynthesis  
144 ( $\varphi_0$ ). The leaf absorptance accounts for the fraction of PAR lost by reflection (albedo),  
145 transmission, and incomplete utilization of the PAR spectrum. We assumed a leaf  
146 absorptance of 0.8 (Collatz et al., 1998) – bearing in mind that this quantity shows  
147 substantial variation among species (Long et al., 1993). The intrinsic quantum  
148 efficiency of photosynthesis is the LUE ( $\text{mol mol}^{-1}$ ) that can be realized at low PAR,  
149 low  $[\text{O}_2]$  and saturating  $[\text{CO}_2]$ . We assigned an intrinsic quantum efficiency of 0.085,  
150 again following Collatz et al. (1998). This is in the mid-range of reported values for  
151 the intrinsic quantum efficiency of  $\text{C}_3$  photosynthesis.

152 As the real atmosphere is not perfectly clear and contains clouds, we considered next  
153 the effect of atmospheric absorption and reflection of PAR.  $\text{PAR}_{\text{toa}}$  for each month of  
154 the year was converted to the PAR incident on vegetation canopies (Table 1) using the  
155 Prescott formula (Linacre, 1968). This modifies GPP by a factor of 0.75 (the clear-sky  
156 transmittivity) under clear skies, declining to 0.25 under completely cloudy skies. The  
157 values thus obtained were increased by 2.7% per km of elevation (Allen, 2005) to  
158 account for the reduced thickness of the atmosphere at higher elevations (Eq. A3).

159 The fraction of absorbed PAR (fAPAR), indicating actual green vegetation cover, was  
160 introduced next. fAPAR is assumed to represent effects of limited water availability,  
161 low temperatures and nutrient deficits in reducing the NPP available for allocation to  
162 leaves as well as the varying phenology and turnover time of leaves (Table 1). It was  
163 further assumed that fAPAR implicitly accounts for the differential penetration of  
164 diffuse and direct PAR into dense vegetation canopies (Mercado et al., 2009). We

165 used the SeaWiFS fAPAR product (1998 to 2004) ([Gobron et al., 2006](#)), which we  
166 have previously used to drive the SDBM in a benchmarking study ([Kelley et al.,  
167 2013](#)). For the present application we averaged different years' values for each month  
168 of the year, to produce a monthly climatology of fAPAR. Missing values in winter  
169 were set to zero. The monthly values of fAPAR were used to multiply the monthly  
170 values of PAR.

171 In the next step the inhibition of CO<sub>2</sub> assimilation at low temperatures was described  
172 by a ramp function, reducing the utilization of PAR for photosynthesis linearly from  
173 10°C to 0°C with zero photosynthesis at daily temperatures below 0°C. Daily values  
174 of PAR were thus integrated over the month to give monthly PAR<sub>0</sub>, as defined in  
175 Table 1. PAR<sub>0</sub> is a weighted monthly PAR, with the weighting provided by the ramp  
176 function (Eq. A4, A5).

177 The final step accounts for the effect of photorespiration and substrate limitation at  
178 subsaturating [CO<sub>2</sub>], based on the Farquhar model (Table 1). GPP was reduced by the  
179 factor  $(c_i - \Gamma^*) / (c_i + 2\Gamma^*)$  where  $\Gamma^*$  is the photorespiratory compensation point. (The  
180 co-limitation hypothesis simply equates the Rubisco- and electron-transport limited  
181 rates of photosynthesis. We use the electron-transport limited rate as this yields an  
182 estimate of LUE. We neglect J<sub>max</sub> limitation, thus making the approximation that  
183 Rubisco is always limiting at high PAR.) The temperature dependence of  $\Gamma^*$  was  
184 described by an Arrhenius function ([Bernacchi et al., 2003](#)), evaluated at the  
185 growing-season mean temperature (mGDD<sub>0</sub>). mGDD<sub>0</sub> is defined as the annual sum of  
186 temperatures above 0°C (growing degree days) divided by the length of the period  
187 with temperatures above 0°C. The ratio  $c_i/c_a$  was predicted as a function of mGDD<sub>0</sub>,  
188 atmospheric aridity ( $\Delta E$ ) and elevation, based on the least-cost hypothesis ([Prentice et  
189 al., 2013](#)).  $\Delta E$  is the cumulative annual difference between actual and equilibrium  
190 evapotranspiration, where actual evapotranspiration is computed using a quasi-daily  
191 soil-moisture accounting scheme ([Cramer and Prentice, 1988](#)). This measure is a  
192 proxy for the effective average value of vapour pressure deficit experienced by the  
193 plants ([Prentice et al., 2013](#)). Further details on the calculation of  $c_i/c_a$  are given in  
194 Sect. A4.

## 195 **2.2 Driving data**

196 PAR, PAR<sub>0</sub>, mGDD<sub>0</sub> and  $\Delta E$  were calculated from insolation and climate data with a  
197 modified version of the STASH model ([Gallego-Sala et al., 2010](#); [Sykes et al., 1996](#)).  
198 STASH was modified to account for the effects of elevation on atmospheric  
199 transmittivity and the effect of atmospheric pressure on the psychrometer constant,  
200 used in the calculation of equilibrium evapotranspiration  
201 (<http://www.fao.org/docrep/X0490E/x0490e07.htm>). The algorithm to compute  
202 insolation was also revised to more accurately compute celestial longitude (the angle  
203 between the Earth's position and its position at the vernal equinox) on each day of the  
204 year, given the orbital parameters (eccentricity, obliquity and precession). The method  
205 of [Kutzbach and Gallimore \(1988\)](#) was used to represent the effect of precession.

206 (This modification has little effect under the present-day orbital configuration.)  
207 Elevations were taken to be the mean elevations of each grid cell as given by CRU  
208 ([http://www.cru.uea.ac.uk/~timm/grid/CRU\\_TS\\_2\\_1.html](http://www.cru.uea.ac.uk/~timm/grid/CRU_TS_2_1.html)). [CO<sub>2</sub>] was set at its mean  
209 value during 1998 to 2005 (370 ppm).

### 210 **2.3 Analysis of annual fAPAR data**

211 We performed an analysis of the controls of (annual) fAPAR. Annual fAPAR was  
212 calculated as a weighted average of the monthly values, the weighting provided by the  
213 mean monthly incident PAR, neglecting periods with mean temperatures below 0°C  
214 (as described in Kelley et al., 2013). We carried out an ordinary linear regression of  
215 fAPAR against the  $\alpha$  coefficient (ratio of actual and equilibrium evapotranspiration)  
216 calculated as in Cramer and Prentice (1988) and Gallego-Sala et al. (2010), modified  
217 as described above. We also performed a generalized linear model analysis using  $\alpha$   
218 and mGDD<sub>0</sub>, then  $\alpha$ , mGDD<sub>0</sub> and total soil cation exchange capacity from the  
219 ISRIC-WISE gridded data set (Batjes, 2009) as predictors of fAPAR.

### 220 **2.4 GPP data-model comparisons**

221 GPP predictions from the final modelling step were compared to the [Luyssaert et al.](#)  
222 [\(2007\)](#) global synthesis of annual GPP measurements from forests. The model's  
223 prediction of global GPP was compared with the range of published, observationally  
224 based estimates ([Beer et al., 2010](#)).

225 Modelled seasonal cycles of GPP were compared with seasonal cycles of gap-filled  
226 GPP derived from eddy covariance measurements of CO<sub>2</sub> exchange in the FLUXNET  
227 archive (<http://www.fluxdata.org/>). One hundred and forty-six flux towers in  
228 FLUXNET have publicly available data between 2002 and 2006. We used all of these  
229 data. Half-hourly measurement pairs of net ecosystem exchange (NEE) and  
230 photosynthetic photon flux density (PPFD) (equivalent to PAR, in photon units) were  
231 partitioned into GPP and ecosystem respiration by fitting the rectangular hyperbola  
232 response model as presented by [Ruimy et al. \(1995\)](#) (their Eq. 27). Non-linear  
233 least-squares regression was performed on each monthly set of NEE-PPFD  
234 observation pairs at each tower, after anomalous data points (identified using Peirce's  
235 criterion) had been deleted. Monthly totals of GPP were then calculated as follows.  
236 First, each PPFD time series was completed using a gap-filling product based on a  
237 half-hourly calculation of solar radiation at the top of the atmosphere, scaled down in  
238 magnitude by daily observations of shortwave downwelling solar radiation as  
239 provided by the WATCH Forcing Data based on the ERA Interim re-analysis  
240 ([Weedon et al., 2012](#)). Then the gap-filled PPFD data were converted to GPP using  
241 the model-fitted parameters for each month and tower, and cumulated to monthly  
242 totals. Months for which the data could not be fitted with a rectangular hyperbola  
243 were excluded from analysis.

## 244 **3 Results**

### 245 **3.1 Model predictions: annual GPP**

246 The patterns and total values of global annual GPP show a progressive reduction  
247 during the course of imposing biophysical and ecophysiological constraints (Fig. 1;  
248 Table 1). Potential GPP based on  $PAR_{toa}$  varies only with latitude, being maximal at  
249 the equator and declining smoothly towards the poles (Fig. 1a). The decline is almost  
250 but not quite symmetrical. The southern hemisphere shows slightly higher values at  
251 any given latitude because the Earth is currently nearest to the Sun in northern winter  
252 (southern summer).

253 The strict latitudinal pattern of potential GPP is altered by cloud cover (Fig. 1b).  
254 Values are lowered around the equator and at high latitudes due to cloudiness. The  
255 highest values are found in subtropical deserts. The combined effects of atmospheric  
256 absorption and clouds reduce total global annual GPP by nearly half (Table 1).

257 The largest drop in modelled GPP, by about 78%, occurs at the next step (Fig. 1c) due  
258 to the introduction of fAPAR. Obvious modifications include the effects of low water  
259 availability in desert regions. fAPAR values of unity are restricted to a very few  
260 locations (e.g. subantarctic islands). Forested regions typically have fAPAR values in  
261 the range 0.2 to 0.8. The moisture indicator  $\alpha$  alone accounted for 45% of the variance  
262 in annual fAPAR. This figure rose to 54% after inclusion of mGDD0 as an additional  
263 predictor, and to 55% after inclusion of soil cation exchange capacity. All three  
264 predictors had highly significant effects ( $P < 0.001$ ).

265 Additional effects of temperature limitation, introduced after the influence of fAPAR  
266 has been taken into account, further diminish GPP only in those regions of the world  
267 (temperate, boreal, polar and high-mountain regions) that routinely experience cold  
268 conditions (Fig. 1d). The reduction in global total annual GPP (Table 1) at this step is  
269 only about 7%.

270 The effects of subsaturating  $[CO_2]$  in limiting GPP are also relatively slight (30%),  
271 but pervasive across terrestrial ecosystems (Table 1). The strongest  $CO_2$  constraint on  
272 GPP is predicted for hot and dry regions such as the Australian deserts; the weakest  
273 constraint is predicted for cold and humid regions, such as eastern Siberia (Fig. 1e).

274 Elevation effects are slight in a global perspective, although significant locally. A  
275 sensitivity test showed that increasing the elevation of the global land surface by 4000  
276 m, with all other factors unchanged, would increase global GPP by 7%. The net effect  
277 is positive because the thinner atmosphere (greater PAR transmission) and reduced  
278 oxygen partial pressure (greater affinity of Rubisco for  $CO_2$ ) at high elevations more  
279 than counteract the negative effects of the reduced psychrometer constant (increased  
280 water loss) and reduced partial pressure of  $CO_2$ .

## 281 3.2 Data-model comparisons: annual GPP

282 The comparison with the Luyssaert et al. observations on annual GPP indicates a  
283 satisfying model prediction at the high end (tropical forests), but a general tendency to  
284 overestimate GPP in temperate and boreal forests (Fig. 2). The predicted global total  
285 GPP value ( $210 \text{ Pg C a}^{-1}$ ) lies above the range of  $123 \pm 8 \text{ Pg C a}^{-1}$  provided by [Beer et](#)  
286 [al. \(2010\)](#) based on eddy covariance flux data and various diagnostic models, and also  
287 above the value of [Welp et al. \(2011\)](#),  $150\text{--}175 \text{ Pg C a}^{-1}$ , inferred from oxygen isotope  
288 data. Nevertheless, inspection of Fig. 2 suggests that the model approximates a  
289 ‘boundary line’ for temperate and boreal forest GPP. A few sites show GPP close to  
290 that modelled, but many others show GPP lower than this. In other words, the model  
291 appears to be predicting an upper bound for GPP, which is not always achieved in the  
292 field. There is no systematic difference between broadleaf and needleleaf forests in  
293 the extent to which the model overpredicts GPP.

## 294 3.3 The seasonal maximum of GPP

295 Although the greatest annual GPP is both predicted and observed for tropical moist  
296 forests (Figs 1, 2), the GPP achieved during the month with maximum GPP can be as  
297 high or higher in boreal or temperate forests. This tendency is shown both by model  
298 predictions (Fig. 3) and flux observations (Fig. 4). Tropical evergreen broadleaf  
299 forests have high GPP throughout the year, with a muted seasonal cycle reflecting the  
300 alternation of wetter and drier seasons (Fig. 4). The estimated average annual GPP of  
301  $2760 \text{ g C m}^{-2} \text{ a}^{-1}$  marks tropical forests as the most productive, but the maximum  
302 monthly GPP in tropical evergreen broadleaf forests (about  $300 \text{ g C m}^{-2} \text{ month}^{-1}$ ) is  
303 exceeded by forests in the temperate zone (Fig. 4). The highest mean monthly GPP  
304 values in our flux data set are  $358 \text{ g C m}^{-2} \text{ month}^{-1}$  in a temperate evergreen needleleaf  
305 forest and  $484 \text{ g C m}^{-2} \text{ month}^{-1}$  in a temperate deciduous broadleaf forest. The  
306 monthly maximum GPP in boreal forests (in June or July), the lower quartile for  
307 temperate deciduous broadleaf forest, and the upper quartile for temperate evergreen  
308 and mixed forests are similar to or even larger than the maximum for tropical  
309 evergreen broadleaf forests.

310 Fig. 3 provides a biophysically based prediction of this phenomenon. In the top panel,  
311 it is already clear that the maximum monthly potential GPP – being proportional to  
312 insolation – is greatest in high latitudes, declining towards the equator. This is  
313 because the day length in high-latitude summer more than compensates for the low  
314 sun angles. The maximum daily insolation at any place and time on the Earth’s  
315 surface occurs near the polar circles in the days around the summer solstice. High  
316 cloud cover (Fig. 3b), low vegetation cover (Fig. 3c) and low temperatures (Fig. 3d)  
317 all tend to reduce the maximum monthly GPP in the Arctic, but the basic pattern  
318 persists (Fig. 3e) even after all constraints are included, allowing high maximum  
319 monthly GPP – comparable to or higher than that in tropical forests – to be achieved  
320 in boreal or temperate forests. The highest values of maximum monthly GPP ( $> 600 \text{ g}$



321 C m<sup>-2</sup> a<sup>-1</sup>) are predicted for certain mid-latitude temperate and boreal forest regions,  
322 including the Caucasus and Altai mountains.

## 323 4 Discussion

### 324 4.1 Key patterns explained

325 Our simple model predicts, among other things, that GPP in the summer months can  
326 be as high as or higher in boreal or temperate forests than it is in tropical forests. This  
327 prediction is supported by flux data (Fig. 4) and consistent with analyses of NPP data  
328 by [Kerckhoff et al. \(2005\)](#) and Huston and Wolverton (2009). Huston and Wolverton  
329 (2009) attributed this pattern to the prevalence of highly weathered, nutrient-poor  
330 soils in the tropics. Our explanation is simpler, based on the latitudinal and seasonal  
331 distribution of insolation and cloud cover combined with the physiology of  
332 photosynthesis. Although it is possible that variations in soil nutrient status are  
333 reflected to some extent in fAPAR (with allocation to leaves being reduced and  
334 allocation to fine roots increased under low-nutrient conditions: [Poorter et al. \(2012\)](#)),  
335 the fact that temperate forests do not consistently have lower fAPAR than tropical  
336 forests suggests that this effect is not predominant; while our analysis of the controls  
337 of fAPAR suggest dominant control by climate, principally water supply, with smaller  
338 contributions from growing-season temperature (reduced fAPAR in cold climates)  
339 and soil properties.

340 We argue therefore that the first-order latitudinal patterns of GPP and its seasonal  
341 cycle are ultimately determined astronomically, by the distribution of insolation. Due  
342 to the obliquity of the Earth's axis relative to the ecliptic, the latitude where the Sun is  
343 directly overhead swings between the Tropics of Cancer and Capricorn, crossing the  
344 equator twice a year. The tropics therefore receive maximum annual insolation. But  
345 the maximum insolation in any one month shows a very different pattern, with highest  
346 values at high latitudes. At latitudes > 50° in both hemispheres the high maximum  
347 monthly insolation is counteracted in its effect on GPP by high cloud cover and  
348 seasonally low temperatures. High incident and absorbed PAR are experienced widely  
349 in summer in boreal and temperate latitudes, resulting in a high seasonal GPP. Our  
350 model is nonetheless consistent with total annual GPP being highest in tropical forests,  
351 due to relatively high insolation combined with adequate temperature and moisture  
352 conditions that persist throughout the year.

353 A novel feature of the model is its inclusion of elevation effects on GPP. Elevation  
354 affects GPP in several ways. Enhanced PAR is a direct result of a reduced path length  
355 through the atmosphere. Reduced stomatal conductance and  $c_i/c_a$  ratios (and  
356 correspondingly higher photosynthetic capacity) are predictions of the least-cost  
357 hypothesis. These predictions have long-standing empirical support ([Friend et al.,](#)  
358 [1989](#); [Körner and Diemer, 1994](#)), but are accounted for here as a consequence of the  
359 reduced partial pressure of O<sub>2</sub>, which lowers the cost of carboxylation relative to

360 transpiration. On the other hand, the reduced psychrometer constant tends to increase  
361  $\Delta E$ . The net effect in our model, *ceteris paribus*, is that GPP increases with elevation.  
362 The global effect is small, but the prediction would be worth exploring in the context  
363 of elevational transects. It has implications especially for primary production in  
364 high-mountain regions in the tropics and subtropics.

## 365 4.2 [CO<sub>2</sub>] and nutrient supply effects

366 We have implicitly assumed that fAPAR is independent of [CO<sub>2</sub>]. Thus, the effect of  
367 the final constraint – where the effect of sub-saturating CO<sub>2</sub> and with it, the effect of  
368 restrictions on  $c_i$  and GPP due to stomatal closure in dry environments, are added –  
369 reflects only the effects of [CO<sub>2</sub>] on the rate of photosynthesis that could be achieved  
370 on the assumption of unchanging vegetation cover. The resulting prediction is a  
371 relatively modest potential for increased GPP with increasing [CO<sub>2</sub>], following the  
372  $A$ - $c_i$  curve for electron transport-limited photosynthesis. A sensitivity analysis in  
373 which [CO<sub>2</sub>] was elevated by 200 ppm yielded a 5% to 25% stimulation of modelled  
374 annual GPP: smaller than the mean effect reported for temperate forest NPP ( $23 \pm 2\%$ )  
375 by [Norby et al. \(2005\)](#) based on Free-Air Carbon dioxide Enrichment (FACE)  
376 experiments. This analysis also suggested a strong relationship between CO<sub>2</sub>  
377 fertilization and temperature with warm areas experiencing stronger CO<sub>2</sub> fertilization.  
378 Annual GPP was predicted to increase by about 18% across the tropics but by no  
379 more than 12% in the high latitudes of both hemispheres. The relationship to  
380 temperature is much less marked than in the analysis by [Hickler et al. \(2008\)](#) because  
381 the LPJ-GUESS model used there did not account for the response of  $c_i/c_a$  to  
382 temperature. In our model, lower  $c_i/c_a$  at lower temperatures implies a strengthening  
383 of the response to  $c_a$  because of the convexity of the  $A$ - $c_i$  curve. This strengthening  
384 partially counteracts the temperature effect on  $\Gamma^*$ , which tends to produce a stronger  
385 CO<sub>2</sub> response at higher temperatures.

386 Additional effects, not considered here, could modify these model predictions. One is  
387 the possible increase of fAPAR resulting from ‘water saving’ by reduced stomatal  
388 conductance at increased [CO<sub>2</sub>]. Evidence has been presented for an increase of  
389 fAPAR, independently of precipitation trends, in warm and dry regions ([Donohue et  
390 al., 2013](#)). Such an increase would also tend to counteract any possible increase in  
391 runoff due to increasing [CO<sub>2</sub>] ([Ukkola and Prentice, 2013](#); [Wang et al., 2012](#)).

392 Another neglected effect is the possible restriction of [CO<sub>2</sub>] fertilization due to  
393 exacerbated nutrient shortages, which would reduce the potential for GPP to be  
394 influenced by [CO<sub>2</sub>]. For example, there is evidence for a decline in CO<sub>2</sub>-induced  
395 growth enhancement over the time scale of stand development in the Oak Ridge  
396 temperate forest FACE experiment (Norby et al., 2010) which appears to be a result  
397 of accelerated N depletion under CO<sub>2</sub> enhancement. On the other hand, a comparative  
398 FACE study of grasslands showed photosynthetic responses to enhanced [CO<sub>2</sub>] to be  
399 independent of N supply (Lee et al., 2011). A possible resolution of apparently  
400 conflicting results on the nutrient dependence of primary production (and by

401 extension, the [CO<sub>2</sub>] effect) would depend on the responses of GPP, NPP and biomass  
402 growth being distinguished (note that NPP includes components such as root  
403 exudation and volatile organic compound emission that do not directly contribute to  
404 biomass growth). Vicca et al. (2012) showed no difference in GPP between forests on  
405 fertile and infertile soils, and no evidence for differences in the NPP/GPP ratio, but a  
406 very large difference in biomass growth – suggesting that the key difference lies in the  
407 allocation of NPP to supporting root symbionts that assist trees in acquiring nutrients  
408 under conditions of low nutrient availability. This finding is consistent with that of  
409 Aoki et al. (2012), who measured many times greater exudation of organic acids from  
410 tropical trees on soils with low P availability, relative to more fertile soils in the same  
411 climate. The effect apparently extends to whole-ecosystem carbon uptake, which was  
412 shown by Fernández-Martínez et al. (2014) to be determined by nutrient availability  
413 to a far greater extent than GPP. These various findings suggest that the current  
414 paradigm for the inclusion of nutrient responses in complex ecosystem models –  
415 whereby nutrient supplies influence photosynthetic rates, and thence NPP and  
416 biomass growth – is incorrect, and that the way forward will involve explicit  
417 modelling of how carbon allocation (to roots *versus* shoots, and to investment in  
418 nutrient acquisition *versus* biomass growth) is influenced by nutrient availability.

### 419 **4.3 Implications for modelling strategy**

420 Global LUE models have a history dating back at least to the early 1990s, with the  
421 publication of the widely used Carnegie-Ames-Stanford Approach model, CASA  
422 ([Field et al., 1995](#); [Potter et al., 1993](#)) and the SDBM ([Knorr and Heimann, 1995](#)) to  
423 predict NPP. Models based on the LUE principle continue to be developed, and  
424 compared, now most commonly in terms of their ability to reproduce GPP as derived  
425 from CO<sub>2</sub> flux measurements (see e.g. Cheng et al., 2014; McCallum et al., 2009,  
426 2013; Verma et al., 2014; Horn and Schulz, 2011; Yuan et al., 2007, 2013). Their  
427 popularity depends on the fact that green vegetation cover in LUE models is directly  
428 provided from satellite observations, thus sidestepping one of the most serious  
429 limitations of current dynamic global vegetation models (DGVMs) – namely their  
430 (in)ability to realistically predict spatial and temporal patterns of green vegetation  
431 cover ([Kelley et al., 2013](#)). Despite persistent differences among different  
432 satellite-derived fAPAR products ([McCallum et al., 2010](#)), the physical definition of  
433 fAPAR is clear, and remotely sensed fAPAR values can be evaluated and ultimately  
434 improved by systematic comparison with *in situ* measurements ([Pickett-Heaps et al.,](#)  
435 [2014](#)).

436 On the other hand, reliable projection of the effects of future [CO<sub>2</sub>] and climate  
437 changes demands that fAPAR also be predicted from first principles. There must be a  
438 feedback from NPP to fAPAR, because sufficient NPP is required to sustain a given  
439 leaf area. Current DGVMs model this feedback implicitly but there has been little  
440 effort to evaluate their predictions of fAPAR and its response to environmental  
441 changes. When tested, models have been found wanting (e.g. Kelley et al. 2013,  
442 Keenan et al. 2014). Process-based prediction of fAPAR is an important goal for

443 further research and presumably a feasible one, given the ready availability of fAPAR  
444 observations as a target.

445 Meanwhile, the multiplicity of available LUE formulations, and the lack of agreement  
446 on (for example) the way temperature and CO<sub>2</sub> responses are built into LUE models  
447 (Verma et al., 2014) or whether or not these responses should be PFT-specific (Yuan  
448 et al., 2013), are causes for concern. These differences ultimately reflect the lack of a  
449 clear theoretical basis for LUE modelling. In this paper, we have attempted to provide  
450 such a basis through the adoption of two optimality hypotheses with independent  
451 empirical support, namely the co-limitation hypothesis (Maire et al., 2012), which  
452 predicts that LUE is determined by the electron-transport limited rate of  
453 photosynthesis according to the Farquhar model, and the least-cost hypothesis  
454 (Prentice et al., 2014), which provides an explicit prediction of  $c_i/c_a$  ratios as a  
455 function of the physical environment. Our model makes the further explicit  
456 assumptions that (a) the controls of LUE are universal in all C<sub>3</sub> plants (thus, we do not  
457 distinguish among PFTs), and (b) soil moisture and nutrient availability constraints on  
458 GPP are mediated by fAPAR and thus do not influence LUE.

459 As a result of these hypotheses and assumptions, the model has far fewer parameters  
460 than most. Aside from constants (such as the intrinsic quantum efficiency of  
461 photosynthesis) that are independently measured to within  $\pm 10\%$  or better, the model  
462 has just one parameter –  $C$  in equation A7 – that has to be estimated (and we have  
463 done this from independent observations). Moreover, the model's explicit relationship  
464 to the Farquhar model of photosynthesis allows a natural way to include the effect of  
465 changes in [CO<sub>2</sub>], requiring no additional parameters to be specified – in contrast with  
466 (for example) Los et al.'s (2013) modification of CASA to include a CO<sub>2</sub> response,  
467 which is otherwise missing from the model.

468 It is commonly impossible to discern the extent to which parameter values in complex  
469 models have been tuned to data that may then be used to evaluate their performance.  
470 However, many models contain 'hidden' parameters whose values are not traceable to  
471 measurements. For example, the temperature response equations of LUE in CASA  
472 (Potter et al., 1993) contain six hard-wired numerical constants, in addition to the  
473 maximum LUE for NPP ( $\epsilon^*$ ) that is explicitly calibrated. The LPJ model (Sitch et al.,  
474 2003) similarly contains PFT-specific temperature 'envelope' responses of unclear  
475 provenance and reliability. This situation reflects the data-poor world into which  
476 models such as CASA and LPJ were born. More recently developed models are often  
477 simpler, with process formulations derived more directly from observations such as  
478 flux measurements. The model presented here represents a further step towards  
479 simplicity and traceability which, we suggest, will be necessary attributes of  
480 'next-generation' ecosystem models.

## 481 **Appendix A**

### 482 **Estimations on the biophysical constraints in the model**

483 **A1 PAR at the top of the atmosphere**

484 Instantaneous solar radiation (insolation) on a horizontal surface at the top of the  
485 atmosphere is given by:

486 
$$Q = Q_{sc} d_r (\sin l \cdot \sin \delta + \cos l \cdot \cos \delta \cdot \cos h)$$
 A1

487 Here,  $Q_{sc}$  is the solar constant ( $1369 \text{ W m}^{-2}$ ) ([Willson and Mordvinov, 2003](#)),  $d_r$  is the  
488 inverse square of the relative Sun-Earth distance (dimensionless),  $l$  is latitude in  
489 radians,  $\delta$  is solar declination in radians, and  $h$  is the 'hour angle' (the time before or  
490 after solar noon, in radians). We use formulae based on the day number to obtain  $d_r$   
491 and  $\delta$ . We assume that over the course of one day there is no variation in  $d_r$  or  $\delta$ . As  
492  $Q_{sc}$  and  $l$  do not vary either, we can obtain daily insolation by integrating with respect  
493 to  $h$  between the hours of sunrise and sunset. The result is:

494 
$$Q = (86400 / \pi) Q_{sc} d_r (h_s \cdot \sin l \cdot \sin \delta + \cos l \cdot \cos \delta \cdot \sin h_s)$$
 A2

495 where  $h_s$  is the hour angle of sunset in the unit of radians, given by  $h_s = \arccos [-\tan l$   
496  $\tan \delta]$ . 86400 is the number of seconds in a day. The term in the square brackets has to  
497 be set to 1 if it exceeds 1, or  $-1$  if it becomes less than  $-1$ , which are the special cases  
498 of polar day and night.

499 Daily total PAR at the top of the atmosphere is taken to be  $0.5 Q$  (in energy units),  
500 which is then converted to quantum units (photosynthetic photon flux density) using  
501 the factor  $4.5 \text{ MJ mol}^{-1}$  (a spectrally averaged value for the energy content of 1 mol of  
502 photosynthetically active photons). Photon units are preferred because photosynthesis  
503 depends on the absorption of a given number of quanta, rather than a given amount of  
504 electromagnetic energy. LUE is thus a dimensionless quantity.

505 **A2 Atmospheric transmissivity and cloud cover**

506 Daily solar shortwave radiation ( $R_{sw\downarrow}$ ) is given by a modification of the Prescott  
507 formula:

508 
$$R_{sw\downarrow} = Q(0.25 + 0.5n_i)(1 + 0.027z)$$
 A3

509 where  $n_i$  is the daily fractional hours of bright sunshine (dimensionless), which we  
510 equate with the one-complement of fractional cloud cover as given in the CRU TS3.1  
511 dataset, and  $z$  is elevation (km) above sea level. The second term in brackets is a  
512 correction for the thinning of the atmosphere with increasing elevation.

### 513 A3 Low-temperature inhibition

514 Low-temperature inhibition of photosynthesis is accounted for by weighting daily  
515 values of PAR ( $PAR_d$ ) in the accumulation of PAR during a month. We denote the  
516 weighted monthly PAR by  $PAR_0$ . The weighting is calculated as follows:

$$517 \quad PAR_{0d} = 0 \quad T_d \leq 0^\circ\text{C}$$

$$518 \quad PAR_{0d} = PAR_d (T_d/10) \quad 0^\circ\text{C} < T_d < 10^\circ\text{C} \quad \text{A4}$$

$$519 \quad PAR_{0d} = PAR_d \quad T_d \geq 10^\circ\text{C}$$

520 where  $T_d$  ( $^\circ\text{C}$ ) is daily temperature, giving

$$521 \quad PAR_0 = \sum_{i=1}^n PAR_{0d} \quad \text{A5}$$

522 where  $n$  is the total number of days in the month.

### 523 A4 Leaf-internal [CO<sub>2</sub>]

524 The ‘least-cost’ hypothesis states that the sum of the unit costs of maintaining  
525 carboxylation and transpiration capacities is minimized. To a good approximation,  
526 this applies when the long-term effective value of  $c_i/c_a$  is given by  $\xi/(\xi + \sqrt{D})$ . Here  $D$   
527 is an annual effective value of the vapor pressure deficit and  $\xi$  is given by  $\sqrt[3]{(bK/1.6a)}$   
528 where  $K$  is the effective Michaelis-Menten coefficient for Rubisco-limited  
529 photosynthesis. The cost factor  $b$  is the (assumed conservative) ratio of leaf  
530 maintenance respiration to Rubisco carboxylation capacity; the cost factor  $a$  is the  
531 ratio of sapwood maintenance respiration to transpiration capacity, which is expected  
532 to vary with sapwood permeability, plant height ( $H$ ), and the dynamic viscosity of  
533 water ( $\eta$ ). We assume that xylem element tapering is perfectly efficient ([West et al.,  
534 1997, 1999](#)) so the costs of maintaining the transpiration pathway vary only linearly  
535 with height (because of the increase in the amount of respiring sapwood) and  
536 conductance does not decline due to increasing path length. Efficient tapering is a  
537 prerequisite of the pipe model ([Shinozaki et al., 1964a, b](#)) that empirically relates  
538 sapwood area and subtended leaf area, independently of path length. Therefore,  $a$  can  
539 be expressed as a product of  $H$ ,  $\eta$  and a reference value of  $a$  ( $a_{ref}$ ), and the equation for  
540 optimum  $c_i/c_a$  can be re-written as:

$$541 \quad \frac{c_i}{c_a} = \frac{1}{1 + \sqrt{\frac{1.6a_{ref}H\eta D}{bK}}} \quad \text{A6}$$

542 We put the constant terms (1.6,  $a_{ref}$  and  $b$ ) together outside the square root and denote  
543 them collectively as  $C$ . Equation A6 can then be simplified to:

$$544 \quad \frac{c_i}{c_a} = \frac{1}{1 + C \sqrt{\frac{H\eta D}{K}}} \quad A7$$

545 Using a satellite-derived global dataset on vegetation height ([Simard et al., 2011](#)), we  
546 performed a multiple regression of  $H$  against  $D$  and *annual*  $PAR_0$  (all three variables  
547 log-transformed) yielding the following relationship between  $H$  and the other two  
548 predictors:

$$549 \quad H = c \cdot PAR_0^{0.46} \cdot D^{-0.21} \quad A8$$

550 This relationship is helpful as it suggest a further simplification of equation A7 to  
551 allow for the compensating effect of reduced vegetation height in more arid climates.  
552 We simply make the approximation  $H \propto D^{-0.25}$ , leading to:

$$553 \quad \frac{c_i}{c_a} = \frac{1}{1 + C \sqrt{\frac{\eta}{K}} \sqrt{D}} \quad A9$$

554 Temperature effects are imposed through the known temperature dependencies of  $\eta$   
555 and  $K$  (Prentice et al. 2013). The variation of  $K$  with elevation takes account of the  
556 effect of  $p_o$  (the partial pressure of oxygen) as  $K = K_c (1 + p_o/K_o)$  where  $K_c$  and  $K_o$  are  
557 the Michaelis-Menten coefficients of Rubisco for carboxylation (in the absence of  $O_2$ )  
558 and oxygenation, respectively.  $p_o$  declines with elevation in proportion to atmospheric  
559 pressure ( $P$ ),

$$560 \quad P = 101.325 e^{-0.114z} \quad A10$$

561 ([Jacob, 1999](#)). We estimated  $C$  based on the common observation that  $c_i/c_a \approx 0.8$  at  
562 low elevations in warm, mesic climates. As a reference case we considered  $z = 0\text{km}$ ,  
563  $mGDD_0 = 18^\circ\text{C}$  and  $\Delta E = 100\text{mm}$  (similar to the environment of Sydney, Australia),  
564 yielding  $C = 14.76$ .

## 565 **Acknowledgments**

566 HW was funded by the Australian Research Council through a Discovery Grant (to  
567 ICP and Ian Wright) “Next-generation vegetation model based on functional traits”

568 (grant no. DP120103600), and TWD by Imperial College under a start-up grant to  
569 ICP. We thank Brad Evans, Trevor Keenan, Vincent Maire, Ning Dong and Ian  
570 Wright for discussions and Brad Evans for helping with the flux partitioning. This  
571 paper is a contribution to the AXA Chair Programme on Biosphere and Climate  
572 Impacts and Imperial College's initiative on Grand Challenges in Ecosystems and the  
573 Environment. This work used Free Fair-Use eddy covariance data acquired by the  
574 FLUXNET community and in particular by the following networks: AmeriFlux (U.S.  
575 Department of Energy, Biological and Environmental Research, Terrestrial Carbon  
576 Program (DE-FG02-04ER63917 and DE-FG02-04ER63911)), AsiaFlux,  
577 CarboEuropeIP, Fluxnet-Canada (supported by CFCAS, NSERC, BIOCAP,  
578 Environment Canada, and NRCan), OzFlux, and TCOS-Siberia. We acknowledge the  
579 financial support to the eddy covariance data harmonization provided by  
580 CarboEuropeIP, FAO-GTOS-TCO, iLEAPS, Max Planck Institute for  
581 Biogeochemistry, National Science Foundation, University of Tuscia, Université  
582 Laval and Environment Canada and US Department of Energy and the database  
583 development and technical support from Berkeley Water Center, Lawrence Berkeley  
584 National Laboratory, Microsoft Research eScience, Oak Ridge National Laboratory,  
585 University of California–Berkeley, University of Virginia.

## 586 **References**

587 Ahlström, A., Schurgers, G., Arneeth, A., and Smith, B.: Robustness and uncertainty in  
588 terrestrial ecosystem carbon response to CMIP5 climate change projections,  
589 *Environmental Research Letters*, 7, 044008, 2012. doi:  
590 10.1088/1748-9326/7/4/044008

591 Allen, R.G., Walter, I.A., Elliott, R. L., Howell T. A., Itenfisu D., Jensen, M. E.,  
592 Snyder, R.L.: *The ASCE Standardized Reference Evapotranspiration Equation*,  
593 Amer. Society of Civil Engineers, Reston, Virginia, 2005

594 Anav, A., Friedlingstein, P., Kidston, M., Bopp, L., Ciais, P., Cox, P., Jones, C., Jung,  
595 M., Myneni, R., and Zhu, Z.: Evaluating the Land and Ocean Components of the  
596 Global Carbon Cycle in the CMIP5 Earth System Models, *Journal of Climate*, 26,  
597 6801-6843, 2013.

598 Aoki, M., Fujii, K., and Kitayama, K.: Environmental control of root exudation of  
599 low-molecular weight organic acids in tropical rainforests, *Ecosystems*, 15,  
600 1194-1203, 2012.

601 Arora, V. K., Boer, G. J., Friedlingstein, P., Eby, M., Jones, C. D., Christian, J. R.,  
602 Bonan, G., Bopp, L., Brovkin, V., and Cadule, P.: Carbon-concentration and  
603 carbon-climate feedbacks in CMIP5 Earth system models, *Journal of Climate*, 26,  
604 5289-5314, 2013.

605 Badawy, B., Rödenbeck, C., Reichstein, M., Carvahalais, N., and Heimann, M.:



606 Technical Note: The Simple Diagnostic Photosynthesis and Respiration Model  
607 (SDPRM), *Biogeosciences*, 10, 6485-6508, 2013.

608 Batjes, N.H.: Harmonized soil profile data for applications at global and continental  
609 scales: updates to the WISE datase, *Soil Use and Management*, 25, 124-127, 2009.

610 Beer, C., Reichstein, M., Tomelleri, E., Ciais, P., Jung, M., Carvalhais, N., Rödenbeck,  
611 C., Arain, M. A., Baldocchi, D., and Bonan, G. B.: Terrestrial gross carbon dioxide  
612 uptake: global distribution and covariation with climate, *Science*, 329, 834-838, 2010.

613 Bernacchi, C. J., Pimentel, C., and Long, S. P.: In vivo temperature response  
614 functions of parameters required to model RuBP-limited photosynthesis, *Plant, Cell &  
615 Environment*, 26, 1419-1430, 2003.

616 Bonan, G. B.: Physiological derivation of the observed relationship between net  
617 primary production and mean annual air temperature, *Tellus B*, 45, 397-408, 1993.

618 Cheng, Y.-B., Zhang, Q., Lyapustin, A. I., Wang, Y., and Middleton, E. M.: Impacts  
619 of light use efficiency and fAPR parameterization on gross primary production  
620 modeling, *Agricultural and Forest Meteorology*, 189-190, 187-197, 2014.

621 Churkina, G. and Running, S. W.: Contrasting Climatic Controls on the Estimated  
622 Productivity of Global Terrestrial Biomes, *Ecosystems*, 1, 206-215, 1998.

623 Ciais, P., Sabine, C., Govindasamy, B., Bopp, L., Brovkin, V., Canadell, J., Chhabra,  
624 A., DeFries, R., Galloway, J., Heimann, M., Jones, C., Le Quéré, C., Myneni, R.,  
625 Piao, S., and Thornton, P.: Chapter6: Carbon and Other Biogeochemical Cycles. In:  
626 *Climate Change 2013 The Physical Science Basis*, Stocker, T., Qin, D., and Platner,  
627 G.-K. (Ed.), 2013.

628 Collatz, G. J., Berry, J. A., and Clark, J. S.: Effects of climate and atmospheric CO<sub>2</sub>  
629 partial pressure on the global distribution of C<sub>4</sub> grasses: present, past, and future,  
630 *Oecologia*, 114, 441-454, 1998.

631 Cramer, W. and Prentice, I.: Simulation of regional soil moisture deficits on a  
632 European scale, *Norsk Geografisk Tidsskrift-Norwegian Journal of Geography*, 42,  
633 149-151, 1988.

634 Del Grosso, S., Parton, W., Stohlgren, T., Zheng, D., Bachelet, D., Prince, S., Hibbard,  
635 K., and Olson, R.: Global potential net primary production predicted from vegetation  
636 class, precipitation, and temperature, *Ecology*, 89, 2117-2126, 2008.

637 DeLUCIA, E., Drake, J. E., Thomas, R. B., and GONZALEZ - MELER, M.: Forest  
638 carbon use efficiency: is respiration a constant fraction of gross primary production?,  
639 *Global Change Biology*, 13, 1157-1167, 2007.

640 Denman, K. L., Brasseur, G., Chidthaisong, A., Ciacis, P., Cox, P. M., Hauglustaine,

641 D., Heinze, C., Holland, E., Jacob, D., Lohmann, U., Ramachandran, S., Da Silva  
642 Dias, P. L., Wofsy, S. C., and Zhang, X.: Couplings Between Changes in the Climate  
643 System and Biogeochemistry. In: *Climate Change 2007: The Physical Science Basis.*  
644 Contribution of Working Group I to the Fourth Assessment Report of the  
645 Intergovernmental Panel on Climate Change, Solomon, S., Qin, D., Manning, M.,  
646 Chen, Z., Marquis, M., Averyt, K. B., Tignor, M., and Miller, H. L. (Eds.), Cambridge  
647 University Press, Cambridge, United Kingdom and New York, NY, USA, 2007.

648 Donohue, R. J., Roderick, M. L., McVicar, T. R., and Farquhar, G. D.: Impact of CO<sub>2</sub>  
649 fertilization on maximum foliage cover across the globe's warm, arid environments,  
650 *Geophysical Research Letters*, 40, 3031-3035, 2013.

651 Farquhar, G., von Caemmerer, S. v., and Berry, J.: A biochemical model of  
652 photosynthetic CO<sub>2</sub> assimilation in leaves of C<sub>3</sub> species, *Planta*, 149, 78-90, 1980.

653 Fatichi, S., Leuzinger, S., and Körner, C.: Moving beyond photosynthesis: from  
654 carbon source to sink - driven vegetation modeling, *New Phytologist*, doi: DOI:  
655 10.1111/nph.12614, 2013. 2013.

656 Fernández-Martínez, M., Vicca, S., Janssens, I. A., Sardans, J., Luysaert, S.,  
657 Campioli, M., Chapin, F. S. III, Ciais, P., Malhi, Y., Obersteiner, M., Papale, D., Piao,  
658 S. L., Reichstein, M., Rodà, F., and Peñuelas, J.: Nutrient availability as the key  
659 regulator of global forest carbon balance, *Nature Climate Change*, 4, 471-476, 2014.

660 Field, C. B., Randerson, J. T., and Malmström, C. M.: Global net primary production:  
661 combining ecology and remote sensing, *Remote Sensing of Environment*, 51, 74-88,  
662 1995.

663 Friedlingstein, P., Cox, P., Betts, R., Bopp, L., Von Bloh, W., Brovkin, V., Cadule, P.,  
664 Doney, S., Eby, M., and Fung, I.: Climate-carbon cycle feedback analysis: Results  
665 from the C4MIP model intercomparison, *Journal of Climate*, 19, 3337-3353, 2006.

666 Friedlingstein, P., Meinshausen, M., Arora, V. K., Jones, C. D., Anav, A., Liddicoat,  
667 S. K., and Knutti, R.: Uncertainties in CMIP5 Climate Projections due to Carbon  
668 Cycle Feedbacks, *J. Climate*, 27, 511–526, 2014.

669 Friend, A., Woodward, F., and Switsur, V.: Field measurements of photosynthesis,  
670 stomatal conductance, leaf nitrogen and  $\delta^{13}\text{C}$  along altitudinal gradients in Scotland,  
671 *Funct. Ecol.*, 1989. 117-122, 1989.

672 Gallego-Sala, A., Clark, J., House, J., Orr, H., Prentice, I. C., Smith, P., Farewell, T.,  
673 and Chapman, S.: Bioclimatic envelope model of climate change impacts on blanket  
674 peatland distribution in Great Britain, *Climate Research*, 45, 151-162, 2010.

675 Garbulsky, M. F., Peñuelas, J., Papale, D., Ardö, J., Goulden, M. L., Kiely, G.,  
676 Richardson, A. D., Rotenberg, E., Veenendaal, E. M., and Filella, I.: Patterns and  
677 controls of the variability of radiation use efficiency and primary productivity across

678 terrestrial ecosystems, *Global Ecology and Biogeography*, 19, 253-267, 2010.

679 Gobron, N., Pinty, B., Aussedat, O., Chen, J. M., Cohen, W. B., Fensholt, R., Gond,  
680 V., Huemmrich, K. F., Lavergne, T., Melin, F., Privette, J. L., Sandholt, I., Taberner,  
681 M., Turner, D. P., Verstraete, M. M., and Widlowski, J.-L.: Evaluation of fraction of  
682 absorbed photosynthetically active radiation products for different canopy radiation  
683 transfer regimes: Methodology and results using Joint Research Center products  
684 derived from SeaWiFS against ground-based estimations, *Journal of Geophysical  
685 Research-Atmospheres*, 111, D13110, 2006. doi: 10.1029/2005JD006511

686 Haxeltine, A. and Prentice, I. C.: BIOME3: An equilibrium terrestrial biosphere  
687 model based on ecophysiological constraints, resource availability, and competition  
688 among plant functional types, *Global Biogeochemical Cycles*, 10, 693-709, 1996.

689 Hickler, T., Smith, B., Prentice, I. C., Mjöfors, K., Miller, P., Arneth, A., and Sykes,  
690 M. T.: CO<sub>2</sub> fertilization in temperate FACE experiments not representative of boreal  
691 and tropical forests, *Global Change Biology*, 14, 1531-1542, 2008.

692 Hoffman, F. M., Randerson, J. T., Arora, V. K., Bao, Q., Six, K. D., Cadule, P., Ji, D.,  
693 Jones, C. D., Kawamiya, M., and Khatiwala, S.: Causes and Implications of Persistent  
694 Atmospheric Carbon Dioxide Biases in Earth System Models, *Journal of Geophysical  
695 Research: Biogeosciences*, 119, 2014. doi:10.1002/2013JG002381

696 Horn, J. E., and Schulz, K.: Identification of a general light use efficiency model for  
697 gross primary production, *Biogeosciences*, 8, 999-1021, 2011.

698 Huston, M. A. and Wolverton, S.: The global distribution of net primary production:  
699 resolving the paradox, *Ecological Monographs*, 79, 343-377, 2009.

700 Jacob, D.: *Introduction to atmospheric chemistry*, Princeton University Press, 1999.

701 Jones, C., Robertson, E., Arora, V., Friedlingstein, P., Shevliakova, E., Bopp, L.,  
702 Brovkin, V., Hajima, T., Kato, E., and Kawamiya, M.: 21st Century compatible CO<sub>2</sub>  
703 emissions and airborne fraction simulated by CMIP5 Earth System models under 4  
704 Representative Concentration Pathways, *Journal of Climate*, 26, 4398-4413, 2013.

705 Keenan, T. F., Gray, J., Friedl, M. A., Toomey, M., Bohrer, G., Hollinger, D. Y.,  
706 Munger, J. W., O'Keefe, J., Schmid, H. P., Wing, I. S., Yang, B., and Richardson, A.  
707 D.: Net carbon uotake has increased through warming-induced changes in temperate  
708 forest phenology, *Nature Climate Change*, 4, 598-604, 2014.

709 Kelley, D. I., Prentice, I. C., Harrison, S. P., Wang, H., Simard, M., Fisher, J. B., and  
710 Willis, K. O.: A comprehensive benchmarking system for evaluating global  
711 vegetation models, *Biogeosciences*, 10, 3313-3340, 2013.

712 Kerkhoff, A. J., Enquist, B. J., Elser, J. J., and Fagan, W. F.: Plant allometry,  
713 stoichiometry and the temperature - dependence of primary productivity, *Global*

714 Ecology and Biogeography, 14, 585-598, 2005.

715 Knorr, W. and Heimann, M.: Impact of drought stress and other factors on seasonal  
716 land biosphere CO<sub>2</sub> exchange studied through an atmospheric tracer transport model,  
717 Tellus B, 47, 471-489, 1995.

718 Körner, C. and Diemer, M.: Evidence that Plants from High Altitudes Retain their  
719 Greater Photosynthetic Efficiency Under Elevated CO<sub>2</sub>, *Funct. Ecol.*, 8, 58-68, 1994.

720 Kutzbach, J. and Gallimore, R.: Sensitivity of a coupled atmosphere/mixed layer  
721 ocean model to changes in orbital forcing at 9000 years BP, *Journal of Geophysical*  
722 *Research: Atmospheres* (1984–2012), 93, 803-821, 1988.

723• Lee, T., Barrott, S., and Reich, P.: Photosynthetic responses of 13 grassland  
724• species across 11 years of free-air CO<sub>2</sub> enrichment is modest, consistent and  
725 independent of N supply, *Global Change Biology*, 17, 2893 - 2904, 2011.  
726

727 Linacre, E.: Estimating the net-radiation flux, *Agricultural meteorology*, 5, 49-63,  
728 1968.

729 Long, S., Postl, W., and Bolhar-Nordenkamp, H.: Quantum yields for uptake of  
730 carbon dioxide in C<sub>3</sub> vascular plants of contrasting habitats and taxonomic groupings,  
731 *Planta*, 189, 226-234, 1993.

732 Los, S. O.: Analysis of trends in fused AVHRR and MODIS NDVI data for 1982-2006:  
733 Indication for a CO<sub>2</sub> fertilization effect in global vegetation, *Global Biogeochemical*  
734 *Cycles*, 27, 318-330, 2013.

735 Luysaert, S., Inglis, I., Jung, M., Richardson, A. D., Reichstein, M., Papale, D.,  
736 Piao, S. L., Schulze, E. D., Wingate, L., Matteucci, G., Aragao, L., Aubinet, M., Beer,  
737 C., Bernhofer, C., Black, K. G., Bonal, D., Bonnefond, J. M., Chambers, J., Ciais, P.,  
738 Cook, B., Davis, K. J., Dolman, A. J., Gielen, B., Goulden, M., Grace, J., Granier, A.,  
739 Grelle, A., Griffis, T., Grünwald, T., Guidolotti, G., Hanson, P. J., Harding, R.,  
740 Hollinger, D. Y., Huttyra, L. R., Kolari, P., Kruijt, B., Kutsch, W., Lagergren, F.,  
741 Laurila, T., Law, B. E., Le Maire, G., Lindroth, A., Loustau, D., Malhi, Y., Mateus, J.,  
742 Migliavacca, M., Misson, L., Montagnani, L., Moncrieff, J., Moors, E., Munger, J. W.,  
743 Nikinmaa, E., Ollinger, S. V., Pita, G., Rebmann, C., Rouspard, O., Saigusa, N., Sanz,  
744 M. J., Seufert, G., Sierra, C., Smith, M. L., Tang, J., Valentini, R., Vesala, T., and  
745 Janssens, I. A.: CO<sub>2</sub> balance of boreal, temperate, and tropical forests derived from a  
746 global database, *Global Change Biology*, 13, 2509-2537, 2007.

747 Maire, V., Martre, P., Kattge, J., Gastal, F., Esser, G., Fontaine, S., and Soussana,  
748 J.-F.: The coordination of leaf photosynthesis links C and N fluxes in C<sub>3</sub> plant species,  
749 *PloS one*, 7, e38345, 2012. doi: 10.1371/journal.pone.0038345

750 McCallum, I., Wagner, W., Schullius, C., Shvidenko, A., Obersteiner, M., Fritz, S.,

751 and Nilsson, S.: Satellite-based terrestrial production efficiency modeling, Carbon  
752 balance and Management, 4, 8, 2009.

753 McCallum, I., Wagner, W., Schullius, C., Shvidenko, A., Obersteiner, M., Fritz, S.,  
754 and Nilsson, S.: Comparison of four global FAPAR datasets over Northern Eurasia  
755 for the year 2000, Remote Sensing of Environment, 114, 941-949, 2010.

756 McCallum, I., Franklin, O., Moltchanova, E., Merbold, L., Schullius, C., Shvidenko,  
757 A., Schepaschenko, D., and Fritz, S.: Improved light and temperature responses for  
758 light-use-efficiency-based GPP models, Biogeosciences, 10, 6577-6590, 2013.

759 Mercado, L. M., Bellouin, N., Sitch, S., Boucher, O., Huntingford, C., Wild, M., and  
760 Cox, P. M.: Impact of changes in diffuse radiation on the global land carbon sink,  
761 Nature, 458, 1014-1017, 2009.

762 Monteith, J. and Moss, C.: Climate and the efficiency of crop production in Britain  
763 [and discussion], Philosophical Transactions of the Royal Society of London. B,  
764 Biological Sciences, 281, 277-294, 1977a.

765 Monteith, J. L. and Moss, C. J.: Climate and the Efficiency of Crop Production in  
766 Britain [and Discussion], Philosophical Transactions of the Royal Society of London.  
767 B, Biological Sciences, 281, 277-294, 1977b.

768 Norby, R. J., DeLucia, E. H., Gielen, B., Calfapietra, C., Giardina, C. P., King, J. S.,  
769 Ledford, J., McCarthy, H. R., Moore, D. J., and Ceulemans, R.: Forest response to  
770 elevated CO<sub>2</sub> is conserved across a broad range of productivity, Proceedings of the  
771 National Academy of Sciences of the United States of America, 102, 18052-18056,  
772 2005.

773 Norby, R. J., Warren, J. M., Iversen, C. M., Medlyn, B. E., and McMurtrie, R. E. CO<sub>2</sub>  
774 enhancement of forest productivity constrained by limited nitrogen availability,  
775 Proceedings of the National Academy of Sciences, 107, 19368-19373, 2010.

776 Pickett-Heaps, C. A., Canadell, J. G., Briggs, P. R., Gobron, N., Haverd, V., Paget, M.  
777 J., Pinty, B., and Raupach, M. R.: Evaluation of six satellite-derived Fraction of  
778 Absorbed Photosynthetic Active Radiation (FAPAR) products across the Australian  
779 continent, Remote Sensing of Environment, 140, 241-256, 2014.

780 Pongratz, J., Lobell, D., Cao, L., and Caldeira, K.: Crop yields in a geoengineered  
781 climate, Nature Climate Change, 2, 101-105, 2012.

782 Poorter, H., Niklas, K. J., Reich, P. B., Oleksyn, J., Poot, P., and Mommer, L.:  
783 Biomass allocation to leaves, stems and roots: meta - analyses of interspecific  
784 variation and environmental control, New Phytologist, 193, 30-50, 2012.

785 Potter, C. S., Randerson, J. T., Field, C. B., Matson, P. A., Vitousek, P. M., Mooney,  
786 H. A., and Klooster, S. A.: Terrestrial ecosystem production: a process model based

787 on global satellite and surface data, *Global Biogeochemical Cycles*, 7, 811-841, 1993.

788 Prentice, I. C., Dong, N., Gleason, S. M., Maire, V., and Wright, I. J.: Balancing the  
789 costs of carbon gain and water transport: testing a new theoretical framework for plant  
790 functional ecology, *Ecology letters*, 17, 82-91, 2013.

791 Ruimy, A., Jarvis, P. G., Baldocchi, D. D., and Saugier, B: CO<sub>2</sub> fluxes over plant  
792 canopies and solar radiation: a review, *Advances in Ecological Research*, 26, 1-68,  
793 1995.

794 Running, S. W., Nemani, R. R., Heinsch, F. A., Zhao, M., Reeves, M., and Hashimoto,  
795 H.: A continuous satellite-derived measure of global terrestrial primary production,  
796 *Bioscience*, 54, 547-560, 2004.

797 Shinozaki, K., Yoda, K., Hozumi, K., and Kira, T.: A quantitative analysis of plant  
798 form-the pipe model theory: I. Basic Analyses, *Jnp. J. Ecol.*, 14, 97-105, 1964a.

799 Shinozaki, K., Yoda, K., Hozumi, K., and Kira, T.: A quantitative analysis of plant  
800 form-the pipe model theory: II. Further evidence of the theory and its application in  
801 forest ecology, *Jpn. J. Ecol.*, 14, 133-139, 1964b.

802 Simard, M., Pinto, N., Fisher, J. B., and Baccini, A.: Mapping forest canopy height  
803 globally with spaceborne lidar, *Journal of Geophysical Research*, 116, G04021, 2011.  
804 doi: 10.1029/2011JG001708

805 Sitch, S., Huntingford, C., Gedney, N., Levy, P., Lomas, M., Piao, S., Betts, R., Ciais,  
806 P., Cox, P., and Friedlingstein, P.: Evaluation of the terrestrial carbon cycle, future  
807 plant geography and climate - carbon cycle feedbacks using five Dynamic Global  
808 Vegetation Models (DGVMs), *Global Change Biology*, 14, 2015-2039, 2008.

809 Sitch, S., Smith, B., Prentice, I. C., Arneth, A., Bondeau, A., Cramer, W., Kaplan, J.  
810 O., Levis, S., Lucht, W., Sykes, M. T., Thonicke, K., and Venevsky, S.: Evaluation of  
811 ecosystem dynamics, plant geography and terrestrial carbon cycling in the LPJ  
812 dynamic global vegetation model, *Global Change Biology*, 9, 161-185, 2003.

813 Sykes, M. T., Prentice, I. C., and Cramer, W.: A bioclimatic model for the potential  
814 distributions of north European tree species under present and future climates, *Journal*  
815 *of Biogeography*, 23, 203-233, 1996.

816 Thomas, R. Q., Zaehle, S., Templer, P. H., and Goodale, C. L.: Global patterns of  
817 nitrogen limitation: confronting two global biogeochemical models with observations,  
818 *Global change biology*, 19, 2986-2998, 2013.

819 Todd-Brown, K., Randerson, J., Post, W., Hoffman, F., Tarnocai, C., Schuur, E., and  
820 Allison, S.: Causes of variation in soil carbon simulations from CMIP5 Earth system  
821 models and comparison with observations, *Biogeosciences*, 10, 1717-1736, 2013.

822 Ukkola, A. and Prentice, I.: A worldwide analysis of trends in water-balance  
823 evapotranspiration, *Hydrology and Earth System Sciences Discussions*, 10,  
824 5739-5765, 2013.

825 Verma, M., Friedl, M. A., Richardson, A. D., Kiely, G., Cescatti, A., Law, B. E.,  
826 Wohlfahrt, G., Gielen, B., Rouspard, O., Moors, E. J., Toscano, P., Vaccari, F. P.,  
827 Gianelle, D., Bohrer, G., Varlagin, A., Buchmann, N., van Gorsel, E., Montagnani, L.,  
828 and Propastin, P.: Remote sensing of annual terrestrial gross primary productivity  
829 from MODIS: an assessment using the FLUXNET La Thuile data set, *Biogeosciences*,  
830 11, 2185-2200, 2014.

831 Vicca, S., Luysaert, S., Peñuelas, J., Campioli, M., Chapin, F. S. III, Ciais, P.,  
832 Heinemeyer, A., Högberg, P., Kutsch, W. L., Law, B. E., Malhi, Y., Papale, D., Piao,  
833 S. L., Reichstein, M., Schulze, E. D., and Janssens, I. A.: Fertile forests produce  
834 biomass more efficiently, *Ecology Letters*, 15, 520-526, 2012.

835 Wang, H., Prentice, I. C., and Ni, J.: Primary production in forests and grasslands of  
836 China: contrasting environmental response of light- and water-use efficiency models,  
837 *Biogeosciences*, 9, 4689-4705, 2012.

838 Waring, R., Landsberg, J., and Williams, M.: Net primary production of forests: a  
839 constant fraction of gross primary production?, *Tree Physiology*, 18, 129-134, 1998.

840 Weedon, G. P., Gomes, S., Balsamo, G., Best, M. J., Bellouin, N., and Viterbo, P.:  
841 WATCH forcing databased on ERA-INTERIM. Retrieved July 24, from  
842 [ftp://rfdata:forceDATA@ftp.iiasa.ac.at](ftp://rfddata:forceDATA@ftp.iiasa.ac.at), 2012.

843 Welp, L. R., Keeling, R. F., Meijer, H. A., Bollenbacher, A. F., Piper, S. C.,  
844 Yoshimura, K., Francey, R. J., Allison, C. E., and Wahlen, M.: Interannual variability  
845 in the oxygen isotopes of atmospheric CO<sub>2</sub> driven by El Niño, *Nature*, 477, 579-582,  
846 2011.

847 West, G. B., Brown, J. H., and Enquist, B. J.: A general model for the origin of  
848 allometric scaling laws in biology, *Science*, 276, 122-126, 1997.

849 West, G. B., Brown, J. H., and Enquist, B. J.: A general model for the structure and  
850 allometry of plant vascular systems, *Nature*, 400, 664-667, 1999.

851 Willson, R. C. and Mordvinov, A. V.: Secular total solar irradiance trend during solar  
852 cycles 21–23, *Geophysical Research Letters*, 30, 1199, 2003.

853 Wright, I. J., Reich, P. B., and Westoby, M.: Least - Cost Input Mixtures of Water  
854 and Nitrogen for Photosynthesis, *The American Naturalist*, 161, 98-111, 2003.

855 Yuan, W., Liu, S., Zhou, G., Zhou, G., Tieszen, L. L., Baldocchi, D., Bernhofer, C.,  
856 Gholz, H., Goldstein, A. H., Goulden, M. L., Hollinger, D. Y., Hu, Y., Law, B. E.,  
857 Stoy, P. C., Vesala, T., and Wofsy, S. C.: Deriving a light use efficiency model from

858 eddy covariance flux data for predicting daily gross primary production across biomes,  
859 *Agricultural and Forest Meteorology*, 143, 189-207, 2007.

860 Yuan, W., Liu, S., Cai, W., Dong, W., Chen, J., Arain, A., Blanken, P. D., Cescatti, A.,  
861 Wohlfahrt, G., Georgiadis, T., Genesio, L., Gianelle, D., Grelle, A., Kiely, G., Knohl,  
862 A., Liu, D., Marek, M., Merbold, L., Montagnani, L., Panferov, O., Peltoniemi, M.,  
863 Rambal, S., Raschi, A., Varlagin, A., and Xia, J.: Are vegetation-specific model  
864 parameters required for estimating gross primary production? *Geoscientific Model*  
865 *Development Discussions*, 6, 5475-5488, 2013.

866

867 Zaehle, S. and Dalmonech, D.: Carbon–nitrogen interactions on land at global scales:  
868 current understanding in modelling climate biosphere feedbacks, *Current Opinion in*  
869 *Environmental Sustainability*, 3, 311-320, 2011.

870



871 **Tables**

872 Table 1. Model equations for each step and the global annual GPP (Pg C a<sup>-1</sup>) estimated  
 873 by each model.

Model equation	Global GPP
$GPP = \varphi_0 \cdot a \cdot PAR_{toa}$	2960
$GPP = \varphi_0 \cdot a \cdot PAR$	1442
$GPP = \varphi_0 \cdot a \cdot PAR \cdot fAPAR$	322
$GPP = \varphi_0 \cdot a \cdot PAR_0 \cdot fAPAR$	300
$GPP = \varphi_0 \cdot a \cdot PAR_0 \cdot fAPAR \cdot \frac{c_i - \Gamma^*}{c_i + 2\Gamma^*}$	210

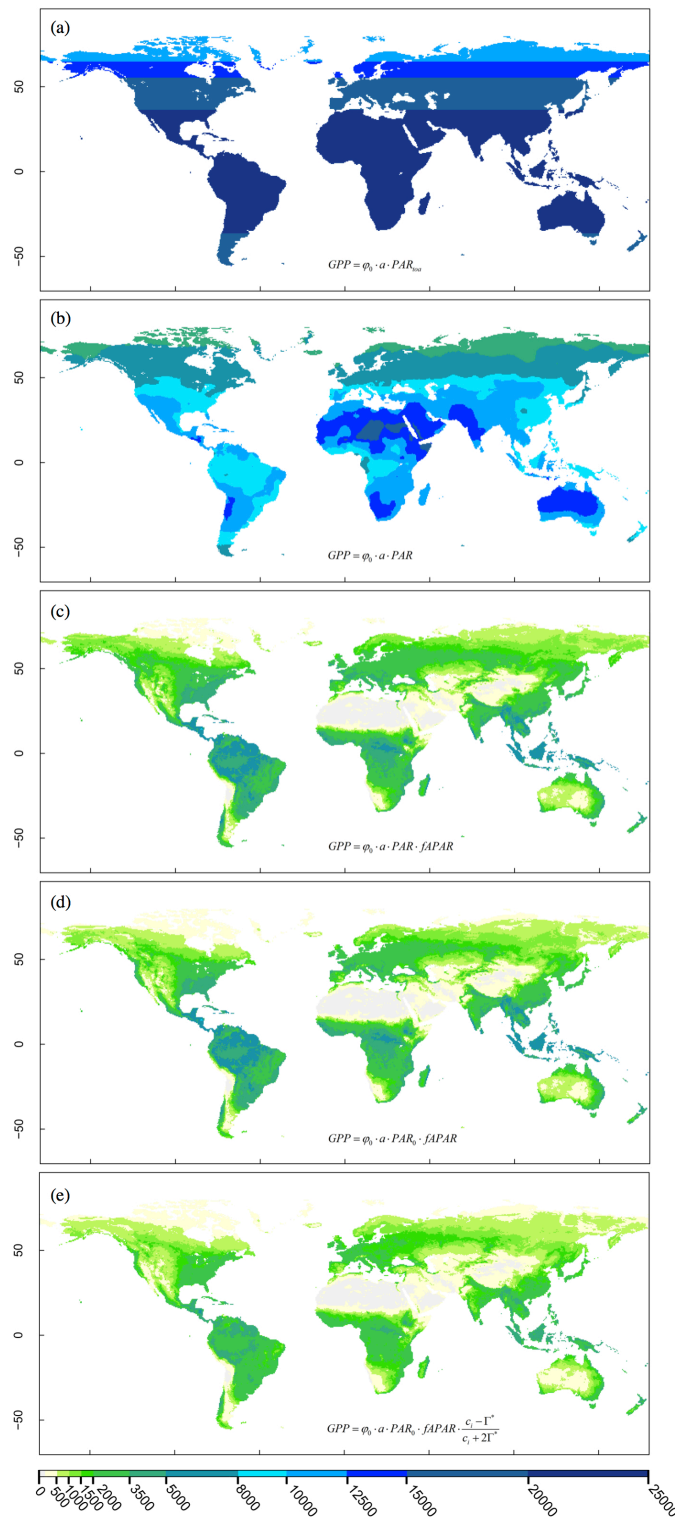
874

875 **Figures**

876 **Figure 1**

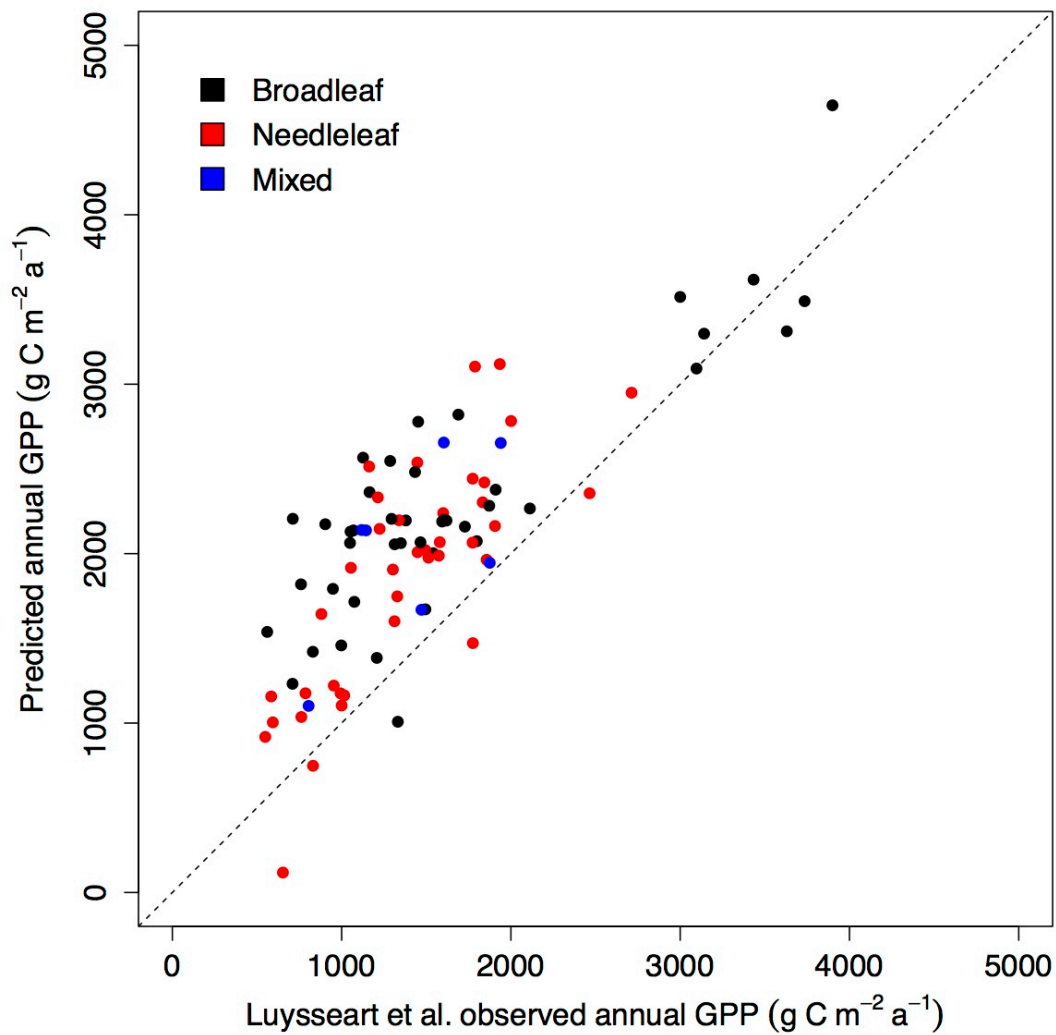
877 The patterns of modelled global annual GPP ( $\text{g C m}^{-2} \text{a}^{-1}$ ) controlled by PAR at the  
878 top of atmosphere (a), and modified by a sequence of effects: atmospheric  
879 transmissivity and cloud cover (b), foliage cover (c), low-temperature inhibition (d)  
880 and  $\text{CO}_2$  limitation (e).

881



882 Figure 2

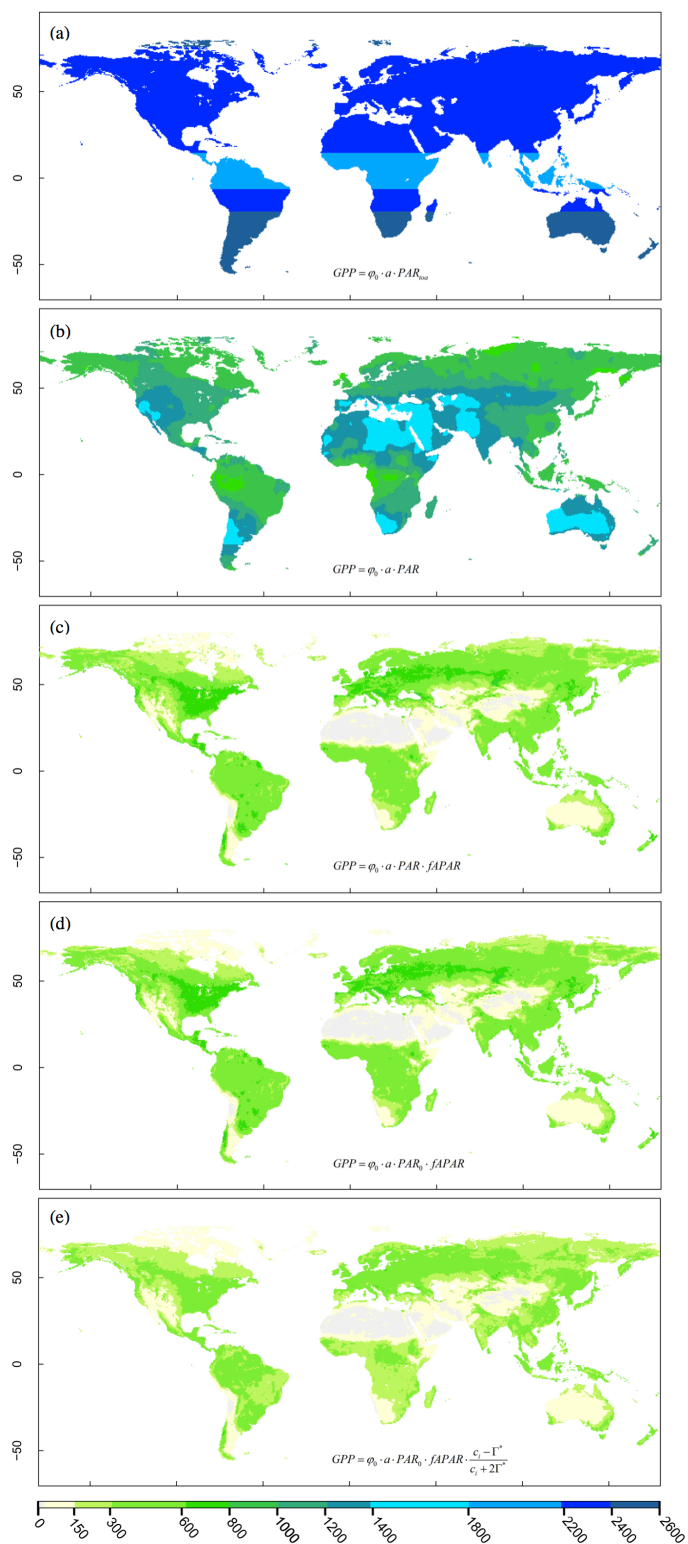
883 Relationship between observed annual GPP from Luysaert et al. (2007) and predicted  
884 annual GPP.



885

886 Figure 3

887 The patterns of modelled global maximum monthly GPP ( $\text{g C m}^{-2} \text{ month}^{-1}$ ) controlled  
888 by PAR at the top of atmosphere and modified by a sequence of effects as in Figure 1.

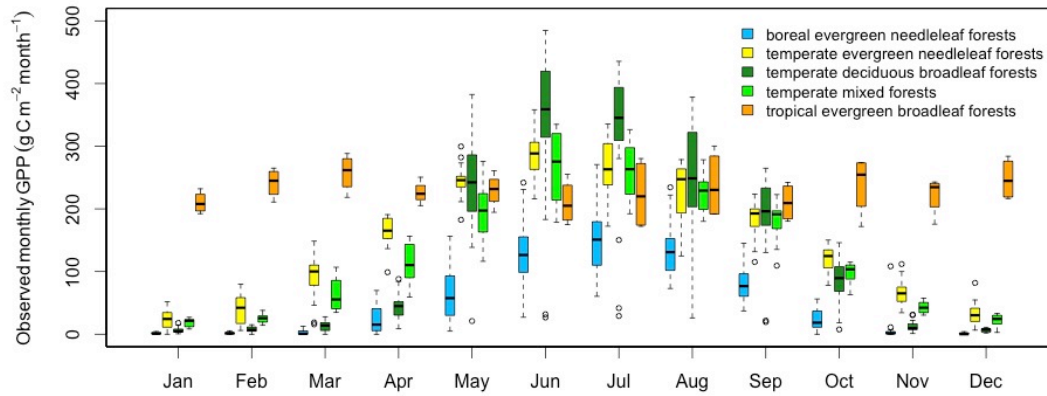


889

890

891 Figure 4

892 Box-and-whisker plot of monthly GPP ( $\text{g C m}^{-2} \text{ month}^{-1}$ ) vs. months, based gap-filled  
893 GPP observations derived from the publicly available measurements in the  
894 FLUXNET archive. The bottom of the box is the lower quartile and the top is the  
895 upper quartile. The whiskers extend to the lower and upper extremes, beyond which  
896 outliers are defined and plotted as dots.



897